Artificial Cytochrome *b*: Computer Modeling and Evaluation of Redox Potentials

Dragan M. Popović,[†] Snežana D. Zarić,[‡] Björn Rabenstein,[†] and Ernst-Walter Knapp*[,†]

Contribution from the Department of Biology, Chemistry, and Pharmacy, Institute of Chemistry, Free University of Berlin, Takustrasse 6, D-14195 Berlin, Germany, and Department of Chemistry, University of Belgrade, Studentski trg 16, P.O. Box, 11001 Belgrade, Yugoslavia

Received November 6, 2000. Revised Manuscript Received April 17, 2001

Abstract: We generated atomic coordinates of an artificial protein that was recently synthesized to model the central part of the native cytochrome b (Cb) subunit consisting of a four-helix bundle with two hemes. Since no X-ray structure is available, the structural elements of the artificial Cb were assembled from scratch using all known chemical and structural information available and avoiding strain as much as possible. Molecular dynamics (MD) simulations applied to this model protein exhibited root-mean-square deviations as small as those obtained from MD simulations starting with the crystal structure of the native Cb subunit. This demonstrates that the modeled structure of the artificial Cb is relatively rigid and strain-free. The model structure of the artificial Cb was used to determine the redox potentials of the two hemes by calculating the electrostatic energies from the solution of the linearized Poisson−Boltzmann equation (LPBE). The calculated redox potentials agree within 20 meV with the experimentally measured values. The dependence of the redox potentials of the hemes on the protein environment was analyzed. Accordingly, the total shift in the redox potentials is mainly due to the low dielectric medium of the protein, the protein backbone charges, and the salt bridges formed between the arginines and the propionic acid groups of the hemes. The difference in the shift of the redox potentials is due to the interactions with the hydrophilic side chains and the salt bridges formed with the propionic acids of the hemes. For comparison and to test the computational procedure, the redox potentials of the two hemes in the native Cb from the cytochrome bc_1 (Cbc_1) complex were also calculated. Also in this case the computed redox potentials agree well with experiments.

Introduction

A large number of enzymes contain redox centers, which can be organic or metal compounds that are important for their function. The redox-active cofactors can be involved in inter- and intramolecular electron transfer (ET) as well as in light-induced charge separation processes. These ET proteins conduct, transport, or donate electrons. Besides the more basic task of a protein matrix to lock the cofactors in a preferred position and orientation to enable or facilitate function, the protein also manages to tune the redox potentials of its cofactors. In this way, an enzyme optimizes the requirements of its function. The same redox-active cofactor can have different values of redox potential, depending on details of protein environment and solvent exposure and thus fulfill different functions in different proteins.

An important subgroup of these ET proteins, the cytochromes, contain one or several hemes. De novo design of such metalloproteins is now possible using modern techniques of peptide synthesis and assembly.[1−5] The production of artificial proteins by modular construction from suitable oligopeptide components avoids the folding problem and does not require an efficient gene expression system. As a consequence, sequence and composition of these artificial proteins can be varied on a much larger scale.[6] Thus, they provide ideal model systems and a test ground to study the factors on which ET processes depend in proteins,[7−14] in DNA,[15,16] and more generally in molecular systems.[17] They also open the possibility to construct artificial

[†] Free University of Berlin.
[‡] University of Belgrade.

(1) Mutter, M.; Altmann, E.; Altmann. K.-H.; Hersperger, R.; Koziej, P.; Nebel, K.; Tuchscherer, G.; Vuilleumier, S. *Helv. Chim. Acta* **1988**, *71*, 835−847.
(2) Robertson, D. E.; Farid, R. S.; Moser, C. C.; Urbauer, J.-L.; Mulholland, S. E.; Pidikiti, R.; Lear, J. D.; Wand, A. J.; DeGrado, W. F.; Dutton, P. L. *Nature* **1994**, *368*, 425−432.
(3) Bryson, J. W.; Betz, S. F.; Lu, H. S.; Suich, D. J.; Zhou, H. X.; O′Neil, K. T.; DeGrado, W. F. *Science* **1995**, *270*, 935−941.
(4) Rabanal, F.; DeGrado, W. F.; Dutton, P. L. *J. Am. Chem. Soc*. **1996**, *118*, 473−474.
(5) Rau, H. K.; Haehnel, W. *J. Am. Chem. Soc*. **1998**, *120*, 468−476.
(6) Rau, H. K.; De Jonge, N.; Haehnel, W. *Angew. Chem., Int. Ed*. **2000**, *39*, 250−253.
(7) Marcus, R. A.; Sutin, N. *Biochim. Biophys. Acta* **1985**, *811*, 265−322.
(8) Onuchic, J. N.; Beratan, D. N.; Winkler, J. R.; Gray, H. B. *Annu. Rev. Biophys. Biomol. Struct.* **1992**, *21*, 349−377.
(9) Moser, C. C.; Keske J. M.; Warncke K.; Farid R. S.; Dutton P. L. *Nature* **1992**, *355*, 796−802.
(10) Dutton, P. L.; Moser, C. C. *Proc. Natl. Acad. Sci. U.S.A.* **1994**, *91*, 10247−10250.
(11) Ullmann, G. M.; Knapp, E. W.; Kostic, N. *J. Am. Chem. Soc*. **1997**, *119*, 42−52.
(12) Zhang, Z.; Huang, L.; Schulmeister, V. M.; Chi, Y.-I.; Kim, K. K.; Hung, L.-W.; Crofts, A. R.; Berry, E. A.; Kim, S.-H. *Nature* **1998**, *392*, 677−684.
(13) Page, C. C.; Moser, C. C.; Chen, X. X.; Dutton, P. L. *Nature* **1999**, *402*, 47−52.
(14) Winkler, J. R.; Di Bilio, A. J.; Farrow, N. A.; Richards, J. H.; Gray, H. B. *Pure Appl. Chem.* **1999**, *71*, 1753−1764.
(15) Lewis, F. D.; Wu, T. F.; Zhang, Y. F.; Letsinger, R. L.; Greenfield, S. R.; Wasielewski, M. R. *Science* **1997**, *277*, 673−676.
(16) Nunez, M. E.; Barton, J. K. *Curr. Opin. Chem. Biol*. **2000**, *4*, 199−206.
(17) Davis W. B.; Svec W. A.; Ratner M. A.; Wasielewski M. R. *Nature* **1998**, *396*, 60−63.

10.1021/ja003878z CCC: $20.00
Published on Web 06/05/2001

proteins that are tailored for specific functions. Artificial ET proteins may be used as photoenzymes capable of light-induced ET,[18] for bioelectronic and biocatalytic applications,[19−21] or as biosensors.[22]

Different structural motives of artificial proteins were designed.[2] Helix−turn−helix peptides were designed, which dimerize into ROP-like,[23] antiparallel four-stranded α-helix bundles.[24,25] The binding of heme to bundles of linear helices was investigated in detail, and maquettes with hemes corresponding to motives from the photosynthetic reaction center, the cytochrome bc_1 complex and the cytochrome *c* oxidase were designed.[2] Recently, the solution structure of an artificially designed four-helix bundle maquette was resolved by NMR spectroscopy.[26] To study ET processes in polypeptide model systems, different cofactors were bound to a single helix,[27] or to bundles of two,[28] three,[29] and four helices.[5]

Cytochrome b (Cb) appears as a component of the membrane-spanning subunit of the mitochondrial cytochrome bc_1 (Cbc_1)[30,31] and the photosynthetic cytochrome b_6f [32] protein complexes, whose functions are the transfer of electrons across the membrane within the protein complex. The central part of the Cb subunit is a four-helix bundle with two hemes axially ligated by two histidines (see Figure 1). With a modular building strategy, a synthetic four-helix bundle protein with two bis-histidine ligated hemes was assembled from templates to model the central part of the native Cb subunit.[5] The functional properties of the artificial Cb are closely related to the redox potentials of the two hemes. The redox potentials of the two hemes from the artificial Cb adopt values of −106 and −170 meV,[5] which are relatively distant from −220 meV, the value of the redox potential of histidine/imidazole coordinated hemes in aqueous solution.[33,34] In contrast to these values, the measurements of the corresponding redox potentials of hemes in the native Cb subunit from the Cbc_1 protein complex adopt still more positive values, +93 and −34 meV.[35−37] Accordingly,

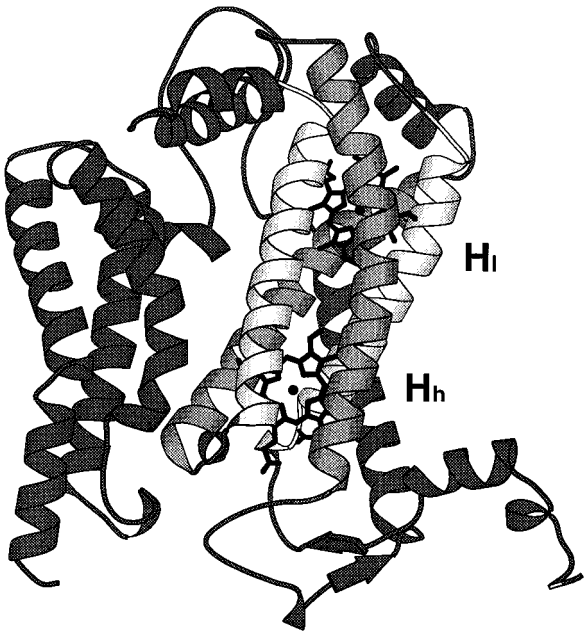

Figure 1. Crystal structure of the C chain of the cytochrome bc_1 complex from bovine heart (Iwata et al., 1998).[31] The four-helix bundle embedding the two hemes is displayed in lighter gray shading. The four-helix bundle of the native Cb is displayed in the same orientation as the artificial Cb (see Figure 2). The two helices corresponding to the helix of type G in the artificial Cb are in light gray, the other two helices of the bundle corresponding to the helices of type F are in darker gray. The low potential heme H_l is in the upper part, the high potential heme H_h is in the lower part of the figure. The figure was generated with MOLSCRIPT (Kraulis, 1991).[67]

the difference in the redox potentials between the high- and low-potential hemes is much larger for the native Cb subunit (127 meV) than for the artificial Cb (70 meV). Although the native and the artificial Cb contain the same cofactors, hemes axially ligated by histidines, the redox potentials of the hemes vary considerably due to differences in the protein environment.

The aim of protein design is to generate novel proteins with tailored structural and functional properties. Here, we developed a procedure to compute observables of artificial proteins from scratch without the availability of a crystal structure. Thus, we open the possibility to understand factors of the protein environment where the observables depend on and thereby provide the basis for a rational design of proteins with desired properties. The artificial Cb protein designed by Rau et al.[5] is a suitable model system to study this approach. A great deal of work was necessary to generate the atomic coordinates of this protein by stepwise sophisticated modeling techniques, taking into account all known structural and chemical knowledge. We believe that with our approach we present a robust and general method to develop "de novo" protein structures. However, since the modeling work is extremely technical and of interest for the specialist, only the procedure is invoked in the main text, while its details are given in the Appendix and Supporting Information of the paper.

To validate the computer-generated structure of the artificial protein, where no crystal or NMR structure is available, characteristic observables must be calculated and compared with measured quantities. We decided here to focus on the redox potential, which is a key parameter of redox active proteins regardless of their involvement in ET reactions. The robustness

(18) Rau, H. K.; De Jonge, N.; Haehnel, W. *Proc. Natl. Acad. Sci. U.S.A.* **1998**, *95*, 11526−11531.
(19) Willner, I.; Heleg-Shabtai, V.; Blonder, R.; Katz, E.; Tao, G.; Brückmann, A. F.; Heller, A. *J. Am. Chem. Soc.* **1996**, *118*, 10321−10322.
(20) Willner, I.; Heleg-Shabtai, V.; Katz, E.; Rau, H. K.; Haehnel, W. *J. Am. Chem. Soc.* **1999**, *121*, 6455−6468.
(21) Katz, E.; Heleg-Shabtai, V.; Willner, I.; Rau, H. K.; Haehnel, W. *Angew. Chem., Int. Ed.* **1998**, *37*, 3253−3256.
(22) Bardea A.; Katz, E.; Brückmann, A. F.; Willner, I. *J. Am. Chem. Soc.* **1997**, *119*, 9114−9119.
(23) Banner, D. W.; Kokkinidis, M.; Tsernoglou, D. *J. Mol. Biol.* **1987**, *196*, 657−675.
(24) Betz, S. F.; DeGrado, W. F. *Biochemistry* **1996**, *35*, 6955−6962.
(25) Betz, S. F.; Liebman, P. A.; DeGrado, W. F. *Biochemistry* **1997**, *36*, 2450−2458.
(26) Skalicky, J. J.; Gibney, B. R.; Rabanal, F.; Bieber-Urbauer, R. J.; Dutton, P. L.; Wand A. J. *J. Am. Chem. Soc.* **1999**, *121*, 4941−4951.
(27) McCafferty, D. G.; Friesen, D. A.; Danielson, E.; Wall, C. G.; Saderholm, M. J.; Erickson, B. W.; Meyer, T. J. *Proc. Natl. Acad. Sci. U.S.A.* **1996**, *93*, 8200−8204.
(28) Kozlov, G. V.; Ogawa, M. Y. *J. Am. Chem. Soc.* **1997**, *119*, 8377−8378.
(29) Mutz, M. W.; McLendon, G. L.; Wishart, J. F.; Gaillard, E. R.; Corin, A. F. *Proc. Natl. Acad. Sci. U.S.A.* **1996**, *93*, 9521−9526.
(30) Xia, D.; Yu, C.; Kim, H.; Xia, J.; Kachurin, A. M.; Zhang, L.; Yu, L.; Deisenhofer, J. *Science* **1997**, *277*, 60−66.
(31) Iwata, S.; Lee, J. W.; Okada, K.; Lee, J. K.; Iwata, M.; Rasmussen, B.; Link, T. A.; Ramaswamy, S.; Jap, B. K. *Science* **1998**, *281*, 64−71.
(32) Martinez, S. E.; Huang, D.; Szczepaniak, A.; Cramer, W. A.; Smith, J. L. *Structure* **1994**, *2*, 95−105.
(33) Wilson, G. S. *Bioelectrochem. Bioenerg.* **1974**, *1*, 172−179.
(34) Moore G. R.; Pettigrew, G. W. *Cytochromes c: Evolutionary, structural and physicochemical aspects*; Springer: Berlin, 1990; pp 309−362.
(35) Hauska, G.; Hurt, E.; Gabellini, N.; Lockau, W. *Biochim. Biophys. Acta* **1983**, *726*, 97−133.
(36) Nelson, B. D.; Gellerfors, P. *Biochim. Biophys. Acta* **1974**, *357*, 358−364.
(37) Nelson, B. D.; Gellerfors, P. *Biochim. Biophys. Acta* **1975**, *396*, 202−209.

of the model structure is probed by monitoring the conformational stability during a long-term simulation of molecular dynamics (MD) and comparing the results with typical values obtained from MD simulations on other proteins where one starts from the crystal structure. To validate our method of calculating redox potentials of hemes independent of the uncertainties of the modeled structure, we decided to calculate the redox potentials also of a heme protein with known crystal structure. As suitable native heme protein we considered Cb from the bovine Cbc_1 membrane protein complex, where a crystal structure is available.[31]

Redox potentials of hemes in proteins were calculated before for the cytochrome *c* subunit of the photosynthetic reaction center from *Rhodopseudomonas viridis*.[38] Here, we used a more detailed charge model of the different redox states of the heme, and we considered the appropriate protonation states of all titratable groups including the propionic acid (PR) groups of the hemes as it was applied by Rabenstein et al.[39,40] for the protonation and redox states of the quinones in the bacterial photosynthetic reaction center and more recently also by Ullmann for cytochrome c_3.[41] We determined the redox potentials by calculating the electrostatic energy differences between hemes in solution and in the appropriate protein environment by solving the linearized Poisson−Boltzmann equation (LPBE).[42−49] The ensemble of protonation and redox patterns of the variably charged groups was then generated with a Monte Carlo (MC) titration method.[50,51]

In this paper we describe the methodologies of modeling that were used to generate the atomic coordinates of the artificial Cb protein and the techniques to evaluate the redox potentials of the hemes. We characterize the generated structure of the artificial Cb, and the calculated redox potentials. The results on the redox potentials provide strong evidence for the relationship between structural characteristics of the protein and the potential in which it can accept or donate electrons. The factors of the protein environment influencing the redox potentials of the hemes and in particular the ones that are responsible for the difference in the redox potentials are investigated by turning on and off specific interaction terms in the artificial Cb.

Methods

In this section we describe the building principles and the construction scheme according to which we generated the atomic coordinates of the artificial Cb protein. Since the build-up of the structure is very technical more details on the construction are given in the Appendix and the Supporting Information. To test the robustness of the structure generated from the artificial Cb, MD simulations of the artificial Cb were compared with those of the native Cb of the mitochondrial Cbc_1 complex from bovine heart, where a crystal structure is available.[31] The steps to prepare the native Cb structure and technical details of the MD simulation are placed in the Supporting Information. To validate the modeled structure of the artificial Cb we calculated the redox potentials of the two hemes of the artificial and native Cb. As necessary information to evaluate the redox potentials we provide the basic theory to calculate electrostatic energies. The atomic charges that we used, the preparation of the structures, and the computational procedures are described in the Supporting Information.

Composition and Building Principles of the Artificial Cytochrome *b*. The artificial protein that we want to study is supposed to mimic structure and function of the native Cb. Both the model protein and the native Cb contain two hemes as cofactors, which are embedded by four helices forming an antiparallel four-helix bundle. The helices of the artificial protein that we study here is held together by a template. The template is a cyclic decapeptide with antiparallel β-sheet structure and two β-turns formed by Pro-Gly residues,[5] whose sequence is given by C A C P G C A C P G. The four-helix bundle is formed by two different types of helices, H_1 with 29 residues and H_2 with 27 residues. They are closely related to the sequence of a maquette introduced by Robertson et al.,[2] to design four-helix bundles. For reasons of notation, we will in the following call helix H_1 containing a phenylalanine at position 15 helix F and helix H_2 containing glycines at positions 8 and 22 helix G. The sequences of helices F (H_1) and G (H_2) are given below:

helix F (H_1):

N-terminus (at template of Cb) C-terminus (at open end of Cb)

```
    1 2 3 4 5 6 7 8 9 0 1 2 3 4 5 6 7 8 9 0 1 2 3 4 5 6 7 8 9
BrAc G G E L R E L H E K L A K Q F E Q L V K L H E E R A K K L NH2
```

helix G (H_2):

N-terminus (at open end of Cb) C-terminus (at template of Cb)

```
    1 2 3 4 5  6 7 8 9 0 1 2 3 4 5 6 7 8 9 0 1 2 3 4 5 6 7
Ac  L E E L W K K G E E L A K K L Q E A L E K G K K L A K NH2
                                                    |
                                                   BrAc
```

(underlined residues are conserved in sequences of Cb from different species)

A model structure of the artificial Cb is displayed in Figure 2. Two pairs of identical helices, F_1, F_2 and G_1, G_2 are placed in opposite corners to form the four-helix bundle, such that helices of the same type are parallel and helices of different type are antiparallel. Helix F contains two histidines, which are used as axial ligands to bind the two hemes. Helix G contains two glycines at the same sequence positions where helix F possesses histidines to accommodate the edges of the bulky hemes. To avoid charged end groups, the C-termini are amidated (NH_2), and the N-termini are acetylated (Ac). However, the N-terminus of helix F and also the side chain of the C-terminal Lys27 of helix G are bromacetylated (BrAc). The bromacetylation is needed to connect these molecular groups by thioether bonds with the cysteines from the template holding the four helices together.

The hemes are located in the binding pocket of the four-helix bundle and axially coordinated by two pairs of histidines attached at the oppositely placed F helices. The heme planes are in parallel orientation. The propionic acid (PR) groups of the hemes point toward the nearest helix ends as in the native Cb. The coordination of the two hemes is stabilized by salt bridges, formed by the negatively charged PR groups and the positively charged arginine residues at positions 5 and 25 of helix G. To isolate the two hemes and to fill the hydrophobic space between them, there is a hydrophobic phenylalanine at residue position 15 in the center of helix G. While the decapeptide template is shielding the high potential heme (H_h) from the solvent, there are two tryptophan residues in position 5 of the helices G to shield the second low-potential heme (H_l) from the solvent.

Except for the four histidines, the artificial protein conserves the interior packing of the hemes by hydrophobic residues. The resulting hydrophobic interactions facilitate the formation of the four-helix bundle. The residues situated on the outer surface of the helix bundle are hydrophilic to increase solubility. The numerous hydrophilic lysines and glutamates at the solvent-exposed surface of the helices allow the formation of salt bridges, which can contribute to the stabilization

(38) Gunner, M. R.; Honig, B. *Proc. Natl. Acad. Sci. U.S.A.* **1991**, *88*, 9151−9155.
(39) Rabenstein, B.; Ullmann, G. M.; Knapp, E. W. *Biochemistry* **1998**, *37*, 2488−2495.
(40) Rabenstein, B.; Ullmann, G. M.; Knapp, E. W. *Biochemistry* **2000**, *39*, 10487−10496.
(41) Ullmann, M. G. *J. Phys. Chem. B* **2000**, *104*, 6293−6301.
(42) Gilson, M. K.; Honig, B. *Biopolymers* **1986**, *25*, 2097−2119.
(43) Nicholls, A.; Honig. B. *J. Comput. Chem.* **1991**, *12*, 435−445.
(44) Davis, M. E.; McCammon, J. A. *J. Comput. Chem.* **1991**, *12*, 909−912.
(45) Bashford, D.; Karplus, M. *J. Phys. Chem.* **1991**, *95*, 9557−9561.
(46) Honig, B.; Nicholls, A. *Science* **1995**, *268*, 1144−1149.
(47) Beroza, P.; Fredkin, D. R.; Okamura, M. Y.; Feher, G. *Proc. Natl. Acad. Sci. U.S.A.* **1991**, *88*, 5804−5808.
(48) Bashford, D.; Gerwert, K. *J. Mol. Biol.* **1992**, *224*, 473−486.
(49) Ullmann, G. M.; Knapp, E. W. *Eur. Biophys. J.* **1999**, *28*, 533−551.
(50) Beroza, P.; Fredkin, D. R.; Okamura, M. Y.; Feher, G. *Biophys. J.* **1995**, *68*, 2233−2250.
(51) Rabenstein, B.; Ullmann, G. M.; Knapp, E. W. *Eur. Biophys. J.* **1998**, *27*, 626−637.

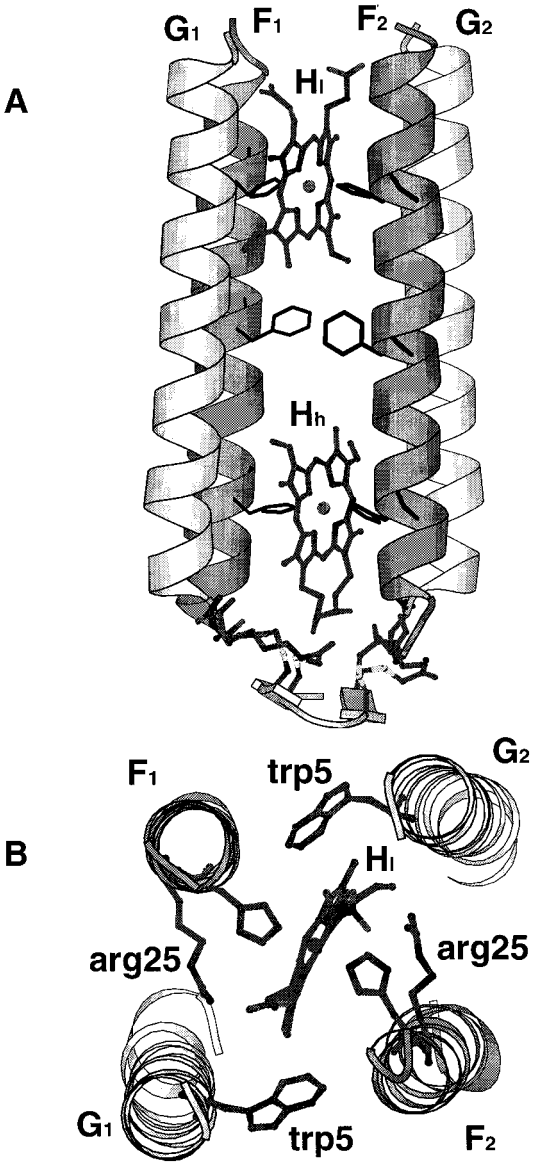

Figure 2. (A) Side view of the artificial Cb. The atomic coordinates were generated by model building and taken after the last step of structural relaxation (see B10 in the Supporting Information). The side view of the artificial Cb is the same as the view of the native Cb displayed in Figure 1. The helices of type F are drawn in darker, the helices of type G in lighter gray. The high potential heme H_h is situated in the lower part of the four-helix bundle. It is shielded from the solvent by a template consisting in an antiparallel cyclic β-strand, which is displayed together with the side chains involved in the four sulfur bridges. The low potential heme H_l is located at the open end of the four-helix bundle (top part). The hemes are displayed together with the histidines His8(F) and His22(F), which are axially ligated to the hemes. The hemes are shielded from each other by a pair of phenylalanines, Phe15(F), which are situated in the center of the figure. (B) Top view of the artificial Cb obtained by model building after the last step of structural relaxation (see B10 in the Supporting Information). The four helices are shown schematically. One can clearly see that the helices of the bundle were slightly distorted and tilted by the process of structural relaxation as compared to the idealized starting structure. For the sake of clarity, the lower part involving the template and the high potential heme is not shown. The low potential heme H_l is displayed together with the axially ligated histidines His22(F_1) and His22(F_2) and the two arginines Arg25(F) forming salt bridges with the PR groups of the low potential heme. Furthermore, the two tryptophanes Trp5(G_1) and Trp5(G_2) shielding the low potential heme at the top of the four-helix bundle from the solvent are shown. The figure was generated with MOLSCRIPT (Kraulis, 1991).[67]

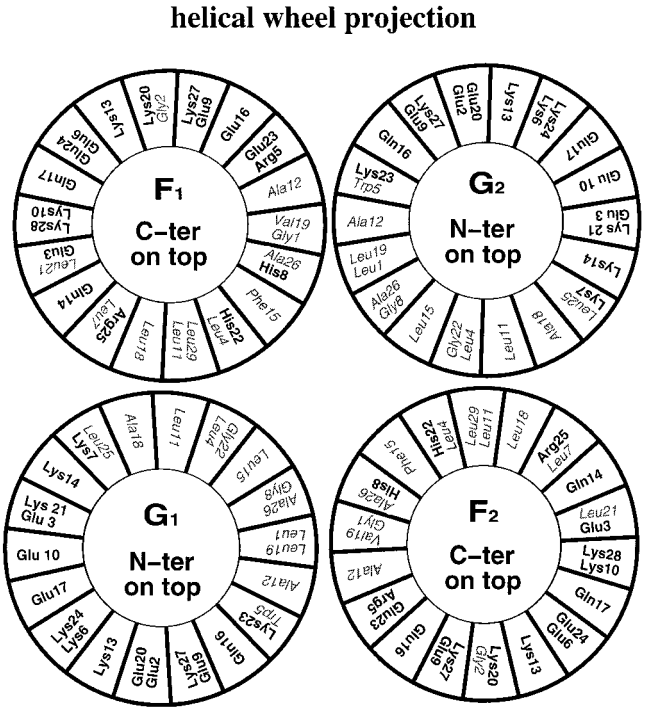

Figure 3. Helical wheel projection of the artificial four-helix bundle viewed from the top. Hydrophobic residues are given by gray shaded, hydrophilic residues by black symbols. Besides the four histidines, only hydrophobic residues are pointing toward the center of the four-helix bundle, thus facilitating the association of the four helices to the helix bundle. On the surface of the four-helix bundle nearly all residues are hydrophilic, which improves the solubility of the artificial Cb. The helices of type F and G correspond to the helices denoted H_1 and H_2 by Rau et al. (1998),[5] respectively.

energy of the α-helices. All of that can be clearly seen from the helical wheel representation of the helices F and G in the four-helix bundle, Figure 3. As a result one obtains a water soluble model protein, where the antiparallel helices shield the heme binding pocket.

Generating Atomic Coordinates of the Artificial Protein by Model Building. A crystal structure of the artificial heme protein is not available yet. However, we could generate atomic coordinates of the artificial protein, since many structural details of the model protein are well established. The coordinates of the 2218 atoms of the artificial Cb were constructed by modeling techniques and constrained energy minimization using the MD program CHARMM22[52,53] with appropriate script files. Albeit, it would have been easier to construct atomic coordinates manually with a graphics program, we preferred this well defined procedure, since it allows repeating individual modeling steps to optimize the resulting structure. Furthermore, the build-up of the molecular structure can only be reproduced, if enough details of the model building process are provided. To obtain a robust and stable model structure, it turned out to be important to avoid strain while building up the structure before structural relaxation. This was achieved by varying the modeling steps iteratively. More details are given in the Appendix. The atomic coordinates of the model structure obtained after the last step of structural relaxation (B10) are available from our webserver with the address: http://lie.chemie.fu-berlin.de/papers/cb1.html.

Computation of the Redox Potentials of Hemes in Proteins. Theoretical Background. The redox potentials of the hemes in the

(52) Brooks, B. R.; Bruccoleri, R. E.; Olafson, B. D.; States, D. J.; Swaminathan, S.; Karplus, M. *J. Comput. Chem.* **1983**, *4*, 187−217.

(53) MacKerell, A. D., Jr.; Bashford, D.; Bellot, M.; Dunbrack, R. L., Jr.; Evanseck, J. D.; Field, M. J.; Fischer, S.; Gao, J.; Guo, H.; Ha, S.; Joseph-McCarthy, D.; Kuchnir, L.; Kuczera, K.; Lau, F. T. K.; Mattos, C.; Michnick, S.; Ngo, T.; Nguyen, D. T.; Prodholm, B.; Reiher, W. E., III; Roux, B.; Schlenkrich, M.; Smith, J. C.; Stote, R.; Straub, J.; Watanabe, M.; Wiórkiewicz-Kuczera, J.; Yin, D.; Karplus, M. *J. Phys. Chem.* **1998**, *102*, 3586−3616.

native and the artificial Cb were determined by averaging over all protonation states of the titratable groups. To obtain the electrostatic energies of the different protonation states, the linear Poisson−Boltzmann equation (LPBE) was solved for the appropriate molecular systems.

$$\vec{\nabla}\cdot[\epsilon(\vec{r})\vec{\nabla}\varphi(\vec{r})] = -4\pi\rho(\vec{r}) + \kappa^2\varphi(\vec{r}) \quad (1)$$

The charge distribution $\rho(\vec{r})$ is given by the atomic partial charges of a given molecular system. The ionic strength is defined through the parameter κ, the inverse Debye length. The electrostatic interaction $G_{i,j}$ of two molecular components i and j whose atoms possess partial charges q^i_m and q^i_n can be computed as

$$G_{ij} = \sum_m q^i_m \varphi^j(\vec{r}^{\,i}_m) \quad (2)$$

where $\varphi^j(\vec{r}^{\,i}_m)$ is the electrostatic potential at position of atom m belonging to molecular group i. Its value is obtained by solving the LPBE (eq 1) with the charge distribution from molecular group j as given below.

$$\rho^j(\vec{r}) = \sum_n q^j_n\, \delta(\vec{r} - \vec{r}^{\,j}_n) \quad (3)$$

Protonation and redox states of the individual variably charged groups depend on each other. The probability $\langle \mathbf{x}_\mu \rangle$ of a variably charged group μ to be protonated or oxidized can be expressed by a thermodynamic average over all 2^N possible charge patterns of the N variably charged groups[49] of the molecular system according to

$$\langle \mathbf{x}_\mu \rangle = \frac{1}{Z}\sum_{n=1}^{2^N} x^{(n)}_\mu \exp(-G^{(n)}/RT) \quad \text{with} \quad Z = \sum_{n=1}^{2^N} \exp(-G^{(n)}/RT) \quad (4)$$

where T is the absolute temperature and R the universal gas constant. For simplicity, we assumed that for each variably charged molecular group only two different charge states are available. However, a generalization is easily possible. The charge state of group μ for the charge pattern (n) is characterized by the integer $x^{(n)}_\mu$, which adopts the value 0 if group μ is unprotonated or reduced (negative charge state) or 1 if protonated or oxidized (positive charge state). The total free energy $G^{(n)}$ of the charge pattern (n) of the considered molecular system is given as

$$G^{(n)} = \sum_{\mu=1}^{N} [x^{(n)}_\mu \Delta G^{\text{intr}}_\mu + \sum_{\nu=1}^{N} x^{(n)}_\mu x^{(n)}_\nu W_{\mu\nu}] \quad (5)$$

The mutual interaction energies $W_{\mu\nu}$ of the titratable groups μ and ν refer to the charge pattern, where all other variably charged groups of the molecular system are unprotonated or reduced, respectively. The interactions of variably charged groups among each other in the unprotonated (reduced) state and with background charges of nonvariably charged groups are accounted for by the intrinsic energy term

$$\Delta G^{\text{intr}}_\mu(\text{pH}) = RT(\text{pH} - \text{p}K^{\text{model}}_{\text{a},\mu}) + (\Delta G^{\text{model}}_{\text{Born},\mu} - \Delta G^{\text{protein}}_{\text{Born},\mu}) + (\Delta G^{\text{model}}_{\text{back},\mu} - \Delta G^{\text{protein}}_{\text{back},\mu}) \quad (6)$$

The first term in eq 6 accounts for the electrostatic free energy of the corresponding titratable group μ, which is used as model compound in solution with known pK_a value. The second term, the so-called Born energy, accounts for the difference in self-energy to protonate (oxidize) the variably charged group μ in the protein and in solution. The last term provides the corresponding energy difference resulting from the interactions of group μ with the background charges. A detailed description of these energy terms can be found in a recent review article.[49] In case the group μ is redox-active, the first term in eq 6 must be replaced by $F(E^{\text{model}}_\mu - E_{\text{sol}})$, where F is the Faraday constant, E_{sol} the redox potential of the solvent and E^{model}_μ the redox potential of the model compound in solution. The total free energy $G^{(n)}$, eq 5, of the charge pattern (n) of the considered molecular system is determined by calculating the electrostatic energies from the solution of the LPBE using Bashford's program MULTIFLEX.[45,48]

Definition of pK_a and redox potential of variably charged groups in protein environment. The free energy difference between the positive and negative charge states of the variably charged molecular group μ depending on pH value and redox potential of the solvent E_{sol} is defined in terms of the ratio of probabilities that this group is charged or uncharged according to

$$\Delta G_\mu(\text{pH}, E_{\text{sol}}) = -RT \ln \frac{\langle \mathbf{x}_\mu \rangle}{1 - \langle \mathbf{x}_\mu \rangle} \quad (7)$$

With this free energy difference, the pK_a value of a titratable group μ in the protein environment can be written as

$$\text{p}K^{\text{protein}}_{\text{a},\mu}(\text{pH}, E_{\text{sol}}) = \text{pH} - \frac{\Delta G_\mu(\text{pH}, E_{\text{sol}})}{RT \ln 10} \quad (8)$$

This expression is related to the sigmoidal Henderson−Hasselbalch titration curve, which describes the dependence of pH on the protonation probability $\langle \mathbf{x}_\mu \rangle$. For a redox-active group μ, the standard redox potential of the group in the protein environment can be written as

$$E^{\text{protein}}_\mu(\text{pH}, E_{\text{sol}}) = E_{\text{sol}} + \frac{\Delta G_\mu(\text{pH}, E_{\text{sol}})}{F} \quad (9)$$

where F is the Faraday constant. It is related to Nernst law, which is the analogue to the Henderson−Hasselbalch titration curve.

Note that for an isolated variably charged group μ, the expressions 8 and 9 are equivalent to the conventional definitions of the p$K_{a,\mu}$ value and the standard redox potential. For several mutually interacting variably charged groups, the free energy difference ΔG_μ in eqs 8 and 9 possesses an implicit pH and E_{sol} dependence besides the trivial dependence for independent variably charged groups, which is RT ln10 [pH − pK^{model}_a] for titratable groups and $F[E^{\text{model}}_\mu - E_{\text{sol}}]$ for redox-active groups. This trivial dependence just takes care that the pK_a and E^0 values are constant for isolated variably charged groups. However, with the generalized definitions 8 and 9, the pK_a value and the standard redox potential E^0 become pH and E_{sol} dependent.[49] Formally one can get rid of these dependencies by defining p$K^{\text{protein}}_{1/2,\mu}$ $E^{\text{protein}}_{1/2,\mu}$ values that are set equal to the pH [E_{sol}] value of the solvent where the probabilities of the charged and uncharged state of the considered variably charged group μ are equal, i.e., at $\langle \mathbf{x}_\mu \rangle = {}^1/_2$ and consequently $\Delta G_\mu = 0$. For an isolated variably charged group these values are equal to the conventional pK_a and E^0 values. The above expressions for pK^{protein}_a(pH, E_{sol}) and the standard redox potential E^{protein}_μ(pH, E_{sol}) may be more useful, if one prefers to characterize the energetics of protonation and redox reactions in proteins in all detail.[41] In this contribution we consider the later definitions but for the artificial Cb also the p$K^{\text{protein}}_{1/2,\mu}$ value is used.

Calculating Protonation and Redox Patterns. The present approach of determining charge patterns of molecular systems is solely based on the computation of electrostatic energies. With this method, no absolute free energies can be obtained.[49] However, energy differences of individual variably charged groups in the protein environment can be evaluated relative to suitable model systems, which serve as a reference. For titratable amino acid side chains, these model systems are the corresponding isolated amino acids in aqueous solution, where the basic and acidic groups of the backbone are acetylated and amidated, respectively. The electrostatic energies for these reference systems were computed in a dielectric medium of $\epsilon_s = 80$ and were matched with the corresponding experimental pK_a values, which are listed for instance by Ullmann and Knapp.[49] For the redox potential of the heme, we used as reference system the bis-histidinyl heme model compound in aqueous solution, where the experimental value of the redox potential is −220 meV.[33]

Inside the protein, the dielectric constant is set to $\epsilon_p = 4$. For a discussion of the choice of this value see for instance the works of Honig and Nicholls,[46] Rabenstein et al.,[51] Warshel et al.[54] For the solvent, we used a dielectric constant of $\epsilon_s = 80$ and an ionic strength

of 100 mM. An ion exclusion layer of 2 Å and a solvent probe radius of 1.4 Å were used.

For the actually considered artificial and native Cb, the number of variably charged molecular groups is too large for a direct evaluation of the Boltzmann averaged sums eq 4. Therefore, we used a Monte Carlo (MC) titration method with Metropolis sampling, for which we used our own program Karlsberg.[39] It is based on the same method as the MCTI program from Beroza et al.[47] but has additional features.[55] The Karlsberg program is freely available under the GNU public license from our web server (http://lie.chemie.fu-berlin.de/karlsberg/).

To improve the sampling efficiency of MC titration, we also use MC moves, where two (three) variably charged groups that couple stronger than 2.5 (5.0) pK_a units change their charge state simultaneously. Such double and triple moves were done in addition to simple moves. A set of MC moves, where it is attempted to change the charge state on the average at all variably charged groups, is called an MC scan. For each MC titration, we performed 1000 full MC scans and after that 10000 reduced MC scans, where all titratable groups that did not change their protonation state after the first 1000 MC scans were fixed in their respective protonation state and excluded from further sampling. This MC titration procedure led to a standard deviation of less than 0.01 protons at each titratable group. We calculated the redox potentials of the hemes in steps of 0.1 pH units varying the pH from 0 to 14, at 300 K and a solution redox potential of $E_{sol} = 0$ mV.

Titratable Groups. All residues known to be titratable were treated as such, regardless of whether they were involved in a salt bridge. The C-termini, the N-termini, the heme propionates (PR), aspartates, glutamates, arginines, lysines, cysteines, tyrosines, and histidines, with the exception of the histidines coordinated to hemes, were considered as titratable groups, while the two hemes (H_l and H_h) of the Cb subunit together with their corresponding imidazole rings were considered as redox-active sites. Note that the PR groups of the hemes were treated as independent titratable groups. In the deprotonated state, nonligating histidines exist in two tautomeric forms. For the native Cb both forms were taken into account in our calculations by representing them as two coupled titratable groups, which cannot simultaneously be deprotonated. In the Cbc_1 complex, there are two additional cofactors with variably charged state. These are the heme of the cytochrome c_1 (Cc_1) subunit and the iron−sulfur cluster from the Rieske subunit. Both were considered to be in the reduced form, because their redox potentials are too high to be oxidized under normal conditions. Furthermore, since the heme of the Cc_1 subunit is more than 35 Å away from the closest heme (H_l) of the Cb subunit, the PR groups of the Cc_1 heme were considered as nontitratable and fixed in their unprotonated state.

Atomic Partial Charges. Using an appropriate set charges is very critical to obtain reliable results for electrostatic energies. Unfortunately, a proper choice of charges is in part a matter of experience. Most of the charges that we use in the present application have been used successfully before to calculate redox potentials of cofactors in proteins.[39,40] Additional charges that were needed for computations of electrostatic energies in this application were computed with procedures that we used in such applications before.

The atomic partial charges of the amino acids, including the charged and neutral states of the titratable residues can be taken from the CHARMM22 parameter set.[53] But, for some of the titratable residues (Arg, Cys, Lys, Tyr, C-ter, N-ter,) only the standard protonation state is available. For this application, we calculated the atomic partial charges of the different protonation states of these residues with the program SPARTAN[56] using the semiempirical PM3 method and the CHELPG procedure, where the charges are determined such that they reproduce the electrostatic potential outside of the considered molecular group appropriately. For the iron sulfur cluster, the charges were taken from Mouesca et al.[57] The pyrrole ring system and the PR groups of the heme were treated as independent variably charged groups that interact electrostatically only. For the atomic partial charges of the propionic acid, the same charges were used as for the side chain of glutamate taken from the CHARMM22[53] parameter set. The complete set of atomic charges used for the different protonation states of all titratable groups can be found in Table S4 of the Supporting Information.

The electronic wave functions of the different redox states of the pyrrole ring system of the heme with two imidazoles as axial ligands without the PR groups were calculated with the Hartree−Fock method from GAUSSIAN98[58] using the 6-31G* basis set for the iron atom and STO-3G basis set for all other atoms. The atomic partial charges were obtained from the wave functions by adjusting the electrostatic potential in the neighborhood of the heme with the Merz−Kollman approach.[59] To reduce the number of independent atomic partial charges, which have to be determined, we constrained the charges of hydrogen atoms bound at CH_2 and CH_3 groups to be equal, except for the hydrogens at the CAA and CAD carbon atoms, where we fixed the charges of two hydrogens at 0.09 and of one at 0.0. In the complete heme, the later hydrogens are replaced by the charge neutral CH_2 groups of the propionic acids. We constrained the charge of the hydrogen atom at the axially ligated imidazole ring that is replaced by the C_β atom of the corresponding histidine to be 0.09. In this way we properly account for the charges at the C_β atom, which together with its two hydrogen atoms possesses a total charge of 0.09.

In these applications it was sometimes observed that the central metal atom carried a negative partial charge.[39] Nevertheless, the calculated electrostatic energies obtained with a charge set with positive charge at the metal yielded practically the same results.[40] The occurrence of negative charges may be due to the large number (in this case 64) of independent charge parameters. It leads to a set of linear equations that is nearly linear dependent, and therefore the charge parameters solving the equations are underdetermined. In the present application we avoided negative charges of the heme iron by fixing the charge of the iron atom to be +0.48 for the oxidized and +0.25 for the reduced bis-histidinyl heme model compound.

Since the calculated atomic charges depend on the orientation of the ligated imidazole rings, the quantum chemical computations were done for all four conformations of the model compound, two of the native Cb and two of the artificial Cb. With this method, we calculated atomic partial charges, which represented the electrostatic potential faithfully in the neighborhood of the bis-histidinyl heme model compound, but provided also the proper values of dipole and quadrupole moments. The atomic partial charges of the bis-histidinyl heme model compound are given in Table S3 of the Supporting Information.

Results and Discussion

In the first part of this section we discuss the structure of the artificial Cb compare it with the native Cb subunit and validate the model structure by studying its structural robustness. In the second part we discuss the results on the redox potentials of the artificial Cb and analyze the factors of the protein environment that determine the redox potentials of the hemes. In the third part we discuss the results on the redox potentials of the native Cb in the Cbc_1 complex of bovine to validate the procedure of calculating redox potentials of hemes in proteins of know structure and compare these results with data from the artificial Cb.

(54) Warshel, A.; Papazyan, A.; Muegge, I. J. *Biol. Inorg. Chem*. **1997**, *2*, 143−152.
(55) Rabenstein, B.; Knapp, E. W. *Biophys. J*. **2001**, *80*, 1141−1150.
(56) *SPARTAN*, version 4.0.; Wavefunction, Inc.: Irvine, CA, 1995.
(57) Mouesca, J. M.; Chen, J. L.; Noodleman, L.; Bashford, D.; Case, D. A. *J. Am. Chem. Soc.* **1994**, *116*, 11898−11914.
(58) Frisch, M. J.; Trucks, G. W.; Schlegel, H. B.; Scuseria, G. E.; Robb, M. A.; Cheeseman, J. R.; Zakrzewski, V. G.; Montgomery, J. A., Jr.; Stratmann, R. E., Jr.; Burant, J. C.; Dapprich, S.; Millam, J. M.; Daniels, A. D.; Kudin, K. N.; Strain, M. C.; Farkas, O.; Tomasi, J.; Barone, V.; Cossi, M.; Cammi, R.; Mennucci, B.; Pomelli, C.; Adamo, C.; Clifford, S.; Ochterski, J.; Petersson, G. A.; Ayala, P. Y.; Cui, Q.; Morokuma, K.; Malick, D. K.; Rabuck, A. D.; Raghavachari, K.; Foresman, J. B.; Cioslowski, J.; Ortiz, J. V.; Stefanov, B. B.; Liu, G.; Liashenko, A.; Piskorz, P.; Komaromi, I.; Gomperts, R.; Martin, R. L.; Fox, D. J.; Keith, T.; Al-Laham, M. A.; Peng, C. Y.; Nanayakkara, A.; Gonzalez, C.; Challacombe, M.; Gill, P. M. W.; Johnson, B.; Chen, W.; Wong, M. W.; Andres, J. L.; Gonzalez, C.; Head-Gordon, M.; Replogle, E. S.; Pople, J. A. *Gaussian 98*, revision A.6; Gaussian, Inc.: Pittsburgh, PA, 1998.
(59) Besler, B. H.; Merz, K. M.; Kollman, P. A. *J. Comput. Chem*. **1990**, *11*, 431−439.

Table 1. Conformation of the Hemes in the Native and Artificial Cytochrome *b*

	Fe−Nϵ2 distance (Å)	Nϵ2−Fe−Nϵ2′ angle[c]	heme and His normal angle[d]	heme normal Nϵ2-middle angle[e]	torsion angle α[f]	torsion angle β[f]	torsion angle γ[f]
			native Cb[a]				
His83	2.08	152.1	68.5	155.8	136.1	−17.4	120.2
	2.06	177.0	82.8	171.6	161.5	−42.3	110.6
	2.03	171.9	95.8	163.0	166.2	−67.0	103.8
His182	2.06		107.1	17.6	112.8	65.6	−168.4
	2.07		83.7	6.4	63.4	106.4	−180.0
	1.98		87.2	9.7	68.9	118.0	−168.0
His97	2.08	171.1	81.5	167.6	5.1	−37.8	−37.1
	2.00	167.8	87.7	177.3	49.5	−83.2	−44.3
	2.07	169.0	108.9	173.6	60.0	−85.0	−39.6
His196	2.06		84.9	9.6	−87.3	72.6	−6.6
	1.99		92.4	7.8	−69.7	62.2	5.9
	2.07		73.2	22.7	−34.2	60.9	34.1
			artificial Cb[b]				
His22(F_1)	2.22	172.1	94.6	161.4	105.2	−101.4	−12.7
	2.11	171.1	91.4	156.6	87.3	−59.9	21.1
His22(F_2)	2.23		78.5	21.3	−120.2	124.1	12.7
	2.21		77.9	4.6	−109.3	93.7	16.6
His8(F_1)	2.17	174.1	107.3	159.2	−45.8	−86.5	−138.9
	2.19	171.6	108.6	163.8	−46.0	−71.0	−121.0
His8(F_2)	2.12		91.2	19.5	86.3	94.0	179.4
	2.10		84.2	13.8	82.5	75.0	168.4

[a] Top values are from the crystal structure of the native Cb; middle values are from the energy minimized X-ray structure of the native Cb; bottom values in brackets are averages from MD simulations. [b] Top values are from the minimized structure of the artificial Cb; bottom values are averages from MD simulations. [c] The bond angle Nϵ2−Fe−Nϵ2′ refers to pairs of histidines axially ligated to the same heme. For the native Cb, the first triplet of values corresponds to the pair His83−His182 and the second triplet of values to His97−His196. For the artificial Cb, the first doublet of values corresponds to His22(F_1)−His22(F_2) and the second doublet of values to His8(F_1)−His8(F_2). Footnotes a and b are valid correspondingly. [d] The vectors Fe−NA, Fe−NB of the heme and the heme normal form a right-handed coordinate system. The same is the case for the vectors Cγ−Cδ and Cγ−Nδ1 of the histidine and the imidazole ring normal. [e] The inclination of the axially ligated imidazole ring with respect to the heme plane is measured by the angle of the heme plane normal with the vector going through atom Nϵ2 and the midpoint of the Cγ−Nδ1 bond (see Figure 4). [f] For a definition of the torsion angles α, β, and γ see Figure 4.

Salt Bridges in the Artificial Cb. We consider an acidic and basic residue pair to form a salt bridge, if the corresponding oxygen−hydrogen distance is less than 4 Å. All four PR groups from the two hemes form strong salt bridges with four arginines inside of the four-helix bundle. From the many possibilities to form salt bridges between glutamates and lysines on the outer helix surfaces, our model of the artificial Cb exhibits only four salt bridges. This is astonishing, since the CHARMM22[53] energy function used to model the atomic coordinates was applied under vacuum conditions, where electrostatic interactions involving salt bridges on a protein surface should be overestimated. These salt bridges are formed by the residue pairs Glu16(F_2)−Lys13(F_2), Glu24(F_2)−Lys28(F_2), Glu20(G_2)−Lys24(G_2), and Glu10(G_1)−Lys14(G_1). Their corresponding oxygen−hydrogen distances are 2.9, 1.7, 2.4, and 3.8 Å, respectively. However, from experiment it is known that solvent exposed salt bridges are generally only marginally stable.

Comparison of Heme Conformations in Artificial and Native Cytochrome *b*. We expect the heme conformations and the interactions of the heme with its axial ligands and the protein environment to be crucial for the values of the redox potential. Therefore, we will compare the differences in the structures of the native Cb taken from the crystal structure of the Cbc_1 complex[31] and of the artificial Cb obtained by modeling procedures. The corresponding structural data are found in Table 1. In the native Cb, the Nϵ2−Fe bond lengths vary for the crystal structure, the energy minimized structure and the average of the MD simulation only between 1.98 and 2.08 Å, which is close to the ideal value of 2.05 Å from the CHARMM22[53] force field. In the artificial Cb, this bond length is slightly larger varying between 2.10 and 2.23 Å. For the artificial Cb, deviations from the ideal bond length remain somewhat larger even after an MD simulation of 1 ns. This may be a hint of some steric interactions in the artificial Cb, which prevent the helices of type F to come closer to the heme.

The Nϵ2−Fe−Nϵ2′ bond angles involving the imidazole nitrogen atoms bound to the heme iron exhibit deviations of about ±10° from the ideal value of 180°, except for the angle involving His83 and His182 of the native Cb with a deviation of almost 30°. But, after energy minimization, that deviation diminishes. By steric effects, the planes of heme and an axially ligated imidazole are expected to be nearly orthogonal, although there is no direct bonded interaction, which would enforce it. Hence, the angle between the normal of the heme plane and the normal of the axially ligated imidazole plane should be about 90°. The largest deviation of 21.5° from 90° can be observed for His83 in the crystal structure of the native Cb, which decreases after energy minimization. Deviations of these angles are generally less pronounced for the artificial Cb, probably because this structure is relaxed by energy minimization more extensively. The angle between the heme plane normal and the vector in the imidazole plane pointing from Nϵ2 to the midpoint of Cγ and Nδ1 (see Figure 4) characterizes the inclination of the imidazole plane with respect to the heme plane in any direction. Due to steric effects also this angle is close to 0° or 180° depending on whether the considered imidazole plane is above (as in Figure 4) or below the heme plane, respectively.

The torsion angles α, β, and γ defined in Figure 4, describe the orientation of the imidazole ring plane with respect to the PR groups of the heme, with respect to the histidine backbone and the orientation of the histidine backbone with the PR groups, respectively.[60] For idealized geometry, where the C_β−C_γ bond of histidine is in the imidazole ring plane, the three torsion angles

(60) Zarić, S. D.; Popović, D. M.; Knapp, E. W. Factors determining the orientation of axially coordinated imidazoles in heme proteins. *Biochemistry* **2001**, in press.

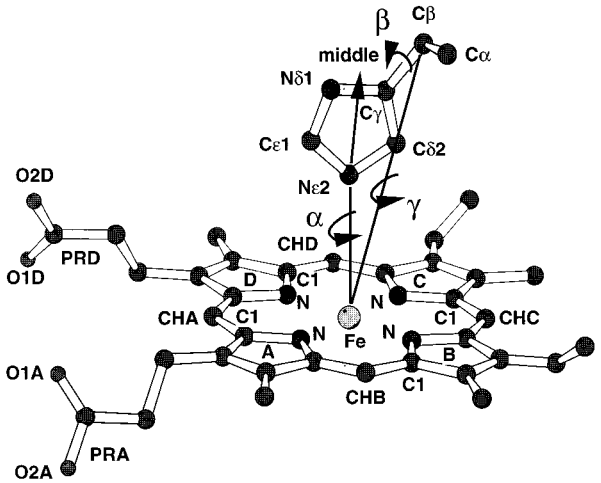

Figure 4. Schematic representation of the heme with its PR groups and one axially ligated histidine. The actual names of the pyrrole ring atoms are obtained by appending the corresponding pyrrole ring label A, B, C, D to the atom names displayed. Note the constituents bound at the pyrrole rings B and C. They are breaking the mirror symmetry with respect to a plane that is orthogonal to the heme plane and goes through the iron and the heme atoms CHA and CHC. The torsion angles α and β, defined in the figure, characterize the orientation of the axially ligated imidazole relative to the PR groups of the heme and relative to the corresponding histidine backbone bond Cα−Cβ, respectively. The torsion angle γ characterizes the orientation of the histidine backbone bond Cα−Cβ relative to the PR groups of the heme. For the shown structure, the values of the torsion angles are about $\alpha \approx 0°$, $\beta \approx 180°$, and $\gamma \approx 180°$. Note that the three torsion angles α, β, and γ depend on each other according to the relation $\gamma = \alpha + \beta$ (Zarić et al., 2001).[60] The figure was generated with MOLSCRIPT (Kraulis, 1991).[67]

Table 2. Relative Orientation of Hemes in Native and Artificial Cb

angles[a]	CHC(H_l)−CHA(H_l) with CHA(H_h)−CHC(H_h)	CHB(H_l)−CHD(H_l) with CHD(H_h)−CHB(H_h)
native Cb[b]	38.2	41.0
	36.8	36.9
	33.7	35.1
artificial Cb[c]	5.0	3.8
	8.9	−14.8

[a] Angles are given in degrees. [b] Top values are from the crystal structure of the native Cb; middle values are from the energy minimized X-ray structure of the native Cb; bottom values in brackets are averages from MD simulations. [c] Top values are from the minimized structure of the artificial Cb; bottom values are averages from MD simulations.

depend on each other and obey the relation $\gamma = \alpha + \beta$. The deviations from this relation encountered here are in the range of only ±1° (see Table 1).

The relative orientation of the two hemes can be measured by the angles between the vectors CHA−CHC (and CHB−CHD) (see Figure 4) belonging to different hemes. By construction, these angles are close to zero for the artificial Cb indicating that the heme planes are mutually parallel and that the PR groups point in opposite directions. The corresponding values are given in Table 2. These preferred orientations relate to the strict regularity of the structure of the artificial Cb, where the helix axes remain nearly parallel also after MD simulation. In the crystal structure of the native Cb the orientations of the helices are not so strictly parallel. Consequently, the relative orientation of the hemes is less regular.

Stability of the Artificial and Native Cb. The robustness of the modeled structure of the Cb can be inferred by observing the structural changes that occur during an MD simulation. The

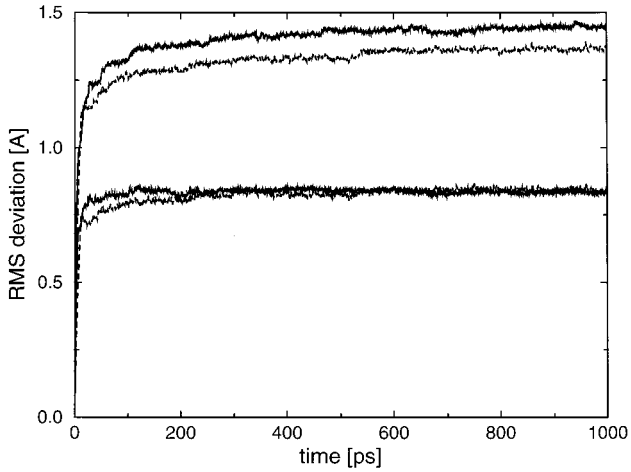

Figure 5. Time evolution of the RMS deviations for the artificial and native Cb. To demonstrate the stability of the structures from the artificial and native Cb, the RMS deviations are displayed as a function of time for 1 ns. The RMS deviations of the backbone atoms without hemes (lower pair of curves) and of all atoms (upper pair of curves). The curves with the slightly smaller values are the data from the native Cb. To remove short time fluctuations in the RMS deviations, averages over 2 ps corresponding to 20 sets of coordinates were displayed. For more details see text.

MD simulations were made under vacuum conditions. For more details refer to the Supporting Information. The time dependencies of the RMS deviations of the atomic coordinates relative to the energy minimized crystal structure of the native Cb and relative to the energy minimized structure of the artificial Cb are shown in Figure 5 for an MD simulation time of 1 ns. Two pairs of lines are depicted in that figure. The upper pair refers to all atoms including hemes and side chains. The lower pair displays the RMS deviations of backbone atoms. For the artificial Cb these are from the four-helix bundle and template only. The RMS deviations of the native Cb are only slightly smaller than of the artificial Cb. After 100 ps, the RMS deviations of the backbone atoms reach a plateau value of 0.85 Å. The RMS deviations of all atoms reach a plateau value of 1.45 Å for the artificial Cb and 1.34 Å for the native Cb. These values of RMS deviations are typical for MD simulations under vacuum conditions applied to crystal structures of relatively stable proteins. Hence, in that respect the model structure of the artificial Cb may be as good as a crystal structure. Comparing the RMS fluctuations of individual Cα atoms obtained from MD simulations of the native Cb with the corresponding values derived from the B factors of the crystal structure, the values from the MD simulations are generally smaller. This result also indicates that the structure of the native Cb is relatively rigid.

Calculated Protonation Pattern of Titratable Groups of the Artificial Cb. Since the redox-active hemes are coupled with all titratable groups in the protein, we calculated the statistical averages of the redox states of the hemes with the protonation states of all titratable groups. At pH = 7 and a solution redox potential of $E_{sol} = 0$, most of the titratable groups adopt standard protonation. Only Arg5(F_1) and PRA(H_h) exhibit considerable deviations from standard protonation behavior (see Figure 6). Their protonation probabilities at pH = 7 and $E_{sol} = 0$ are 0.916 and 0.654, respectively. The propionate PRA(H_h) possesses a higher p$K_{a1/2}$ value than PRA(H_l) and starts to get deprotonated just below pH = 6. This may be due to the salt bridge of PRA(H_h) with Arg5(F_1), which is slightly weaker than the corresponding salt bridge involving

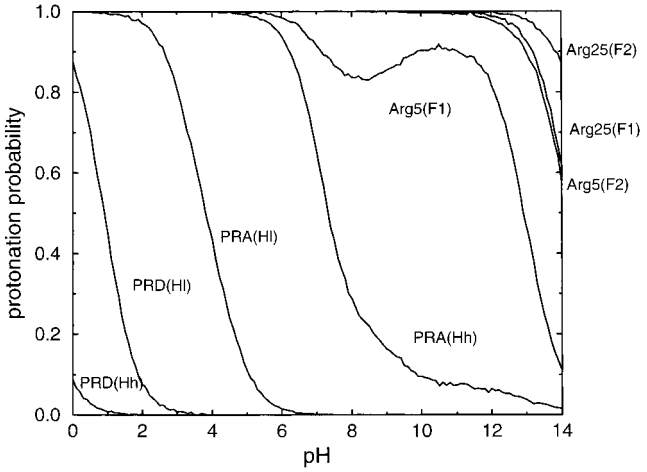

Figure 6. Protonation probability of the four arginines and propionates of the hemes in the artificial Cb as a function of pH at $E_{sol} = 0$. The PR groups are denoted according to the pyrrole ring of heme where they are attached to (A or D) and the heme where they belong to: H_h for high and H_l for low redox potential. The four arginines Arg5(F_1), Arg5(F_2), Arg25(F_1), and Arg25(F_2), whose titration curves are plotted, form salt bridges with PRA(H_h), PRD(H_h), PRA(H_l), and PRD(H_l), respectively. The corresponding O−H distances between the PR groups and the arginines are 2.4 Å, 1.6, 2.1, and 1.5 Å.

PRA(H_l), and due to the interaction of the positively charged Lys23(G_1) and Lys23(G_2), which are close to PRA(H_h) and may weaken its salt bridge. In the pH range of 7 to 12, Arg5(F_1) exhibits an nonmonotonic titration behavior. In the same pH range the titration curve of PRA(H_h) exhibits a plateau. Both is probably due to a strong electrostatic interaction between Arg5(F_1) and PRA(H_h), which are involved in a salt bridge.

Experimental Values of Redox Potentials of Artificial and Native Cb. The redox potentials of the two hemes were measured by observing the differences in the absorbance at the α-band (560 nm) of the hemes as a function of the ambient redox potential of the solvent.[5] Two distinct midpoint redox potentials of −106 meV and −170 meV with standard deviation of ±8 meV were found by fitting the absorbance data to two independent equally weighted terms from Nernst equation. For other synthetic four-helix bundles containing one bis-histidine ligated heme[61] or two noninteracting hemes,[2] the redox potentials are close to the value of −220 meV,[33] found for hemes with axially ligated imidazoles in solution. These synthetic four-helix bundles were formed by a single type of helix maquette, consisting mainly of hydrophilic residues and no arginines to form salt bridges with the PR groups of the hemes. Hence, it was concluded that redox potentials of hemes in a hydrophilic protein environment and without salt bridges involving the PR groups are close to the solution value.[5]

Considering the sequence similarity of the artificial and the native Cb, the high potential heme H_h should be near to the open end and the low potential heme H_l near to the template.[5] Alternatively, one may argue that the heme near the template is better shielded from the solvent and should therefore possess a higher value of the redox potential than the one at the open end. A reliable assignment of the high and low potential hemes in the artificial Cb was possible by orienting the four-helix bundle with the open ends of the two G helices fixed at a gold electrode and observing the voltage dependence of the current of the ET from the gold electrode to the artificial heme in a time-resolved experiment.[20] By this method, the redox potentials of the two hemes close to the open end and close to the template were measured to be −188 and −118 meV, respectively. Hence, with regard to the sequence similarity, the high and low potential hemes in the artificial Cb are exchanged with respect to the native Cb. By analyzing our computations we will show below which factors of the protein environment are shifting the redox potentials.

The values of the redox potentials from the two hemes in the cytochrome b_6f complex at pH = 7, which are −45 and −150 meV,[62] or −50 and −170 meV,[63] are the closest to the values found for the artificial Cb. The two hemes in the Cb subunit of the Cbc_1 complex from bovine heart[31] have with +93 and −34 meV at pH = 7 more positive values of the redox potential.[36]

Calculated Redox Potentials of the Hemes in the Artificial Cb. As has been pointed out in the method section, we used expression 9 to determine the redox potentials. It contains the electrostatic free energy difference ΔG_μ between the reduced and oxidized state of the redox-active group μ, which depends on pH and solvent redox potential E_{sol}. The experimental and the corresponding calculated values of the redox potentials of the hemes in the artificial Cb are collected in Table 3. The redox potentials obtained by evaluating the difference in the electrostatic energies between the solvent and protein environment solving the LPBE resulted in values of −91 meV for the heme near to the template and −167 meV for the heme near to the open end of the four-helix bundle. Those calculated values are very close to the experimental redox potentials of the artificial Cb in solution, which are −106 meV and −170 meV.[5] However, they differ form the values obtained for the artificial Cb attached to a gold electrode, where the corresponding values are −118 and −188 meV.[20] These deviations are presumably due to the different dielectric boundary. The pH dependence of the redox potentials of the hemes in the artificial Cb is shown in Figure 7a.

Hemes possess the same two substituents (−CH_3 and −CH_2−CH_3) at the pyrrole rings B and C, but they bind in a different pattern (see Figure 4). In this way, they violate a possible mirror symmetry with respect to the plane that goes through the atoms CHA and CHC and is orthogonal to the heme plane. The orientation of the two hemes relative to each other, which we consider for most of our computations to evaluate the redox potentials of the hemes from the artificial Cb, corresponds to that found in the native Cb. However, there is no experimental evidence that only this conformation is assumed in the artificial Cb. An alternative conformation of the two hemes is obtained by changing the relative orientation of the hemes in the artificial Cb by rotating one of the hemes by 180° around the virtual bond CHA−CHC. The values of the calculated redox potentials obtained for that "non-native" conformation of the hemes in the artificial Cb are −90 and −162 meV exhibiting only minor changes. Since the substituents are both nonpolar, this result is not surprising.

Electrostatic Coupling of the Hemes. The role of the two phenylalanines Phe15(F) in shielding the redox potentials of the two hemes can be probed by replacing them by two alanines. The resulting shifts in the redox potentials are small. Hence, the cavities with a dielectric constant of $\epsilon = 80$ created by removing the phenyl rings have about the same effect on the redox potential as the phenyl rings themselves. However, the phenyl rings may serve as insulator to reduce the ET rate between the two hemes.

(61) Choma, C. T.; Lear, J. D.; Nelson, M. J.; Dutton, P. L.; Robertson, D. E.; DeGrado, W. F. *J. Am. Chem. Soc.* **1994**, *116*, 856−865.

(62) Hurt, E.; Hauska, G. *J. Bioenerg. Biomembr.* **1982**, *14*, 405−424.

(63) Kramer, D. M.; Crofts, A. R. *Biochim. Biophys. Acta* **1994**, *1184*, 193−201.

Table 3. Redox Potentials of Hemes in Artificial Cb in meV at pH = 7 and E_{Sol} = 0 meV

	heme, H_h near template	heme, H_l near open end	average shift[a]	difference
experimental values				
Rau and Haehnel, 1998 [5 b]	−106	−170	+82	+64
Willner et al., 1999[20]	−118	−188	+67	+70
bis-histidine ligated heme in solution[33,34]	−220	−220	0	0
computed values				
full model with native heme conformation[c]	−91	−167	+91	+76
full model with non-native heme conformation[c]	−90	−162	+94	+72
full model with uncoupled hemes[d]	−100	−176	+82	+76
contributions from different parts by setting atomic charges to zero for				
all residues	−178	−182	+40 (44)[e]	+4 (5)[f]
backbone	−142	−211	+43.5 (48)	+69 (90)
template with links[g]	−95	−167	+89 (98)	+72 (95)
inner hydrophobic side chains[h]	−101	−168	+85.5 (94)	+67 (88)
outer hydrophilic side chains[h]	−92	−129	+109.5 (120)	+37 (49)
all four Arg and PR[i]	−140	−178	+61 (67)	+38 (50)

[a] Average shift of the redox potentials relative to the solution value according to eq 10. [b] The assignment of the measured high and low redox potentials to the two hemes was not certain from the original experiment (Rau and Haehnel, 1998).[5] In the table the assignment was made in agreement with more recent experiments (Willner et al., 1999)[20] and the present computational results. [c] The native heme conformation corresponds to the relative orientation of the hemes as it is in the native Cb, where the hemes can be matched after two 180° rotations, one around the virtual bond CHA−CHC and a second around CHB−CHD. Omitting the second rotation operation corresponds to the non-native heme conformation. For more information, see point A4 of the generation of atomic coordinates in the Supporting Information. If not otherwise stated, the native heme conformation is used. [d] The redox states of the two hemes are uncoupled by calculating the electrostatic energies for the redox state of one heme by fixing the redox state of the other heme in the uncharged reduced state. [e] Fraction in % of the calculated average shift of redox potentials referring to the calculated value of 91 meV. [f] Fraction in % of the calculated difference of redox potentials referring to the calculated value of 76 meV. [g] The links to the template involve the residues Gly1(F_1), Gly1(F_2) and Lys27(G_1), Lys27(G_2). [h] The inner hydrophobic and outer hydrophilic side chains are defined as in Figure 3, but excluding the arginines and histidines. [i] The four arginines, which form salt bridges with the PR groups of the hemes, are Arg5(F_1), Arg5(F_2) and Arg25(F_1), Arg25(F_2).

It is also of interest to investigate to what extent the couplings of the redox states of the two hemes can influence each other. For that purpose, we considered only one of the two hemes is redox-active, while the other remains in its reduced uncharged redox state. However, the calculated difference in the redox potentials between the coupled and uncoupled hemes is small (see Table 3).

Influence of Dielectric Medium and of Charges on the Calculated Redox Potentials. To get a rough idea about the influence of the atomic charges on the redox potentials of the hemes, we set the charges of all residues in the artificial Cb to zero. The calculated redox potentials of the two hemes become very similar and their values are shifted toward the corresponding value −220 meV in aqueous solution (Table 3). The remaining differences of 42 and 38 meV relative to the solution redox potential are due to the low dielectric medium inside of the four-helix bundle protein that is left even after removing all atomic charges. Albeit the effect is very small, the redox potential of the heme H_l near to the open end of the four-helix bundle is somewhat closer to the solution value than the redox potential of the heme H_h, which is near to the template and therefore better shielded from the solvent. The calculated contribution from the low dielectric of the protein volume to the average shift

$$\Delta E_{sol} = \frac{1}{2}[E(H_l) + E(H_h)] - E_{sol} \qquad (10)$$

of the redox potentials of the two hemes $E(H_l)$ and $E(H_h)$ is 44% of the total average shift of ΔE_{sol}(total) = 91 meV. Hence, the remaining 56% of the overall shift is due to the charge distribution in the artificial Cb. These relative contributions are given in Table 3 lower part as percent in brackets.

Removing the atomic charges of the protein backbone, the difference in the redox potentials of the two hemes remains almost the same. However, the difference of the redox potential of the low potential heme to the corresponding value in aqueous solution shrinks to less than 10 meV. From these results, it can be concluded that the charges of the backbone contribute about 52% (the complement to 48%) to the total average shift of the redox potentials of the hemes. The influence of the atomic charges of the template on the redox potentials of the hemes can be tested by setting these charges to zero. No significant change in redox potentials could be observed (see Table 3).

Influence of Different Residue-Types on the Redox Potentials. Next, we consider the effect of different residue types on the shift of the redox potentials. Turning off all atomic charges of the hydrophobic side chains in the interior of the four-helix bundle has only a small effect on the shifts of the redox potentials. This is not surprising, since the corresponding charges are small. On the other hand, turning off the atomic charges of the charged and polar side chains of the outer surface of the four-helix bundle (excluding the arginines and the axially ligated histidines) has a large effect. Surprisingly, the charges of the hydrophilic side chains seem to have practically no effect on the high potential heme at the better shielded closed end of the four-helix bundle, whereas the redox potential of the low potential heme shifts by 38 meV to a higher value more distant to the solvent redox potential. Consequently, the charges of the hydrophilic side chains contribute more than 50% to the difference of the redox potentials. At the same time, these charges exhibit a small but remarkably negative contribution of 20% to the shift of the redox potentials averaged over both hemes.

Finally, we consider the influence of the salt bridges of the PR groups of the heme with the arginines Arg5 and Arg25 of the two F helices. Turning off the corresponding atomic charges, one obtains redox potentials of −140 meV for the heme near the template and of −178 meV for the heme near the open end (Table 3). Accordingly, the charges of the four salt bridges with their corresponding molecular groups contribute 50% to the difference in the redox potentials of the two hemes and 33% to the overall shift of the redox potentials relative to the solution value. The salt bridges of the PR groups with the arginines give

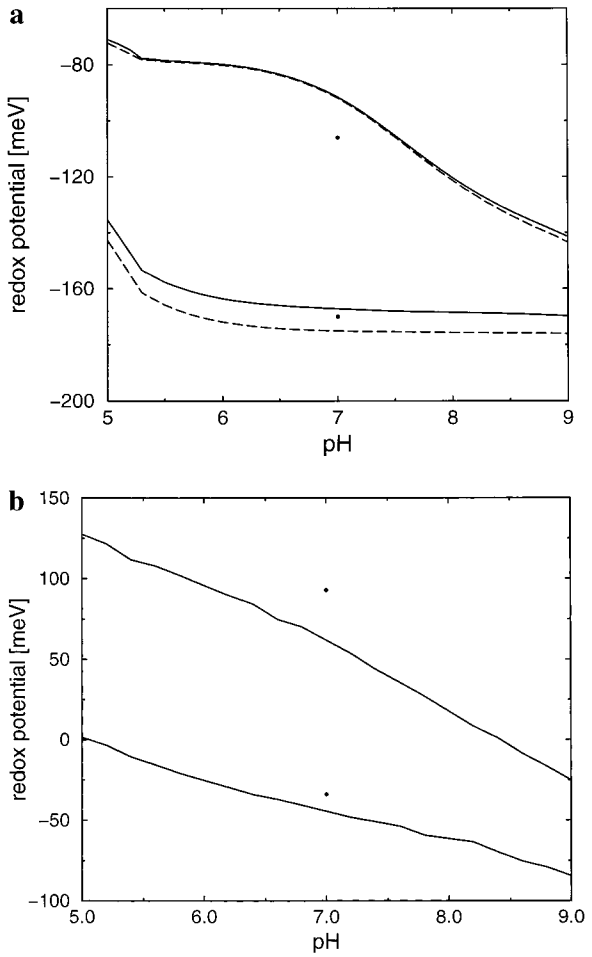

Figure 7. a: pH dependence of the redox potential of the two hemes in the artificial Cb. The experimental values are given by the dots. The pH dependence of the redox potential of the two hemes is displayed in the physiological relevant pH regime from 5 to 9. The redox potentials were evaluated as E_{μ}^{0}(pH, $E_{sol} = 0$) (solid lines) according to eq 9 and as $E_{1/2,\mu}$ value (dashed lines), see method section for more details. Upper curves provide data for the high potential heme H_h close to the template, lower curves for the low potential heme H_l near the open end of the four helix-bundle. b: pH dependence of the redox potential of the two hemes in the native Cb subunit. The experimental values are given by the dots. The pH dependence of the redox potentials of the two hemes is displayed in the physiological relevant pH regime from 5 to 9. The redox potentials were evaluated as E_{μ}^{0}(pH, $E_{sol} = 0$), see method section for more details.

rise to a much stronger shift of the redox potential for the heme near the template (H_h) than for the heme close to the open end (H_l). That is not surprising, since buried salt bridges are generally stronger than solvent exposed salt bridges.

Redox Potentials of the Hemes in the Native Cytochrome *b*. The reliability of the computation of redox potentials of cofactors in proteins generally depends on the quality of the atomic coordinates, on the atomic charges, and on the computational procedure used to obtain the results. In more conventional applications, the atomic coordinates are taken from a crystal structure. Since no crystal structure was available for the artificial Cb, the atomic coordinates were obtained by a modeling procedure, whose quality cannot directly be assessed. To test the reliability of the atomic charges and of the computational procedure separately, we also calculated the redox potentials of the hemes in a native Cb. For that purpose, we used the coordinates from the bovine heart Cbc_1 complex,[31] obtained at pH = 6.6 at 3.0 Å resolution.

Protonation Pattern of Titratable Groups in the Native Cb. Besides the PR groups, only a small number of titratable groups of the native Cb subunit deviate from their standard protonation state in the physiological pH range from 6 to 8 and at a solvent redox potential $E_{sol} = 0$, where the high potential heme (H_h) is reduced, and the low potential heme (H_l) oxidized. For the H_l heme, the PRD(H_l) group is nearly protonated, whereas the PRA(H_l) group is nearly deprotonated. The PR groups of the H_h heme are protonated more symmetrically. There, both PR groups carry together one proton and exhibit only a mild pH dependence.

The titratable groups of the native Cb subunit with nonstandard protonation (protonation probability in brackets) are: Asp254 (0.39), Asp331 (1.00), Glu162 (0.24), Glu202 (0.06), Glu271 (0.99), Lys227 (0.68), N-terminus (0.045), PRA(H_l) (0.045), PRD(H_l) (0.96), PRA(H_h) (0.64) and PRD(H_h) (0.32). The number of groups in the whole bc_1 complex, which possess nonstandard protonation is of course much larger. The protonated titratable group Glu271 is only 3.4 Å away from the of the heme H_l (closest atom HMA1), or 5.4 Å away from the O1A atom of heme H_l. Interestingly, this Glu271 is located in a hydrophobic pocket formed by Pro270, Phe128, Phe274, which can explain the fact that it is protonated.

In contrast to the PR groups of the high potential heme H_h, the protonation pattern of the PR groups at heme H_l is very asymmetric. This can be explained by the salt bridges formed between the PR groups and arginines and by additional interactions with the local protein environment. Arg80 forms a strong salt bridge with PRA(H_l) (O−H distance 2.08 Å), and only a very weak salt bridge (O−H distance 3.8 Å) with the second PR group PRD(H_l) at the same heme. Furthermore, the later PR group is surrounded by several hydrophobic residues (Leu51, Tyr55, Val66 and Pro134) and does not form an H-bond. The PR group PRA(H_h) from heme H_h also forms a strong salt bridge with Arg100 (O−H distance 1.99 Å) and a weak salt bridge (O−H distance 3.2 Å) with the other propionate PRD(H_h). But, in contrast to the corresponding PR group of heme H_l this PR group of heme H_h is in addition to the salt bridge also involved in two H-bonds with the amide hydrogen of Asn206 (O−H distance 1.90 Å), and the hydroxyl hydrogen of Ser106 (O−H distance 2.57 Å). In summary, the electrostatic interactions of the PR groups of heme H_h are more symmetric than the one of heme H_l.

Experimental Values of the Redox Potentials of Hemes in Native Cb. The redox potentials of hemes in native Cb differ considerably from the value in aqueous solution (Table 4). The individual values of the redox potentials of the Cb subunit from the Cbc_1 complex vary for bovine and *Rhodobacter sphaeroides*, while the difference in redox potentials between low and high potential hemes remains at about 120 meV. Even for the functionally analogous but nonhomologous cytochrome b_6f complex from chloroplasts of plants, the difference is the same. For this protein complex, the individual values of the redox potential of the hemes (Table 4) are much closer to those found in the artificial Cb (Table 3). The values of the redox potentials of the hemes from the Cbc_1 complex of bovine exhibit a significant pH dependence in the physiological range decreasing by about 40 meV from pH = 7− 8.[64,65] For the native Cb subunit isolated from the Cbc_1 complex of bovine the differ-

(64) Von Jagow, G.; Scheagger, H.; Engle, W. D.; Machleidt, W.; Machleidt, I. *FEBS Lett.* **1978**, *91*, 121−125.

(65) Von Jagow, G.; Engle, W. D.; Scheagger, H.; Machleidt, W.; Machleidt, I. *Vectorial reactions in electron and ion transport in mitochondria and bacteria*; Palmieri, F., Quagliarello, E., Siliprandi, N., Slater, E. C., Eds.; Elsevier/North-Holland: Amsterdam, 1981; pp 149−161.

Table 4. Redox Potentials of Hemes in Native Cb at Different pH in meV

experimental values	high potential heme	low potential heme	difference
bovine heart mitochondrial cytochrome bc_1 complex[a]	+93	−34	+127
Cb isolated from bovine heart cytochrome bc_1 [b]	−5	−85	+80
Rhodobacter sphaeroides cytochrome bc_1 complex[c]	+50	−60	+110
cytochrome b_6f from chloroplasts[d]	−50	−170	+120
	−45	−150	+105
computed values from cytochrome bc_1 complex	at pH 6.6, 7.0, 8.0	at pH 6.6, 7.0, 8.0	at pH 6.6, 7.0, 8.0
whole complex in solution ($\epsilon = 80$)	+75, +61, +19	−37, −45, −62	+112, +106, +81
Cb from C chain only in solution ($\epsilon = 80$)	+46, +35, −1	−42, −52, −67	+88, +87, +66
Cb from C chain only embedded in membrane[e]	+106, +91, +42	+22, 0, −52	+84, +91, +94

[a] Measured at pH = 7.0, (Nelson et al., 1976).[36] [b] Measured at pH = 7.0, (Von Jagow et al., 1978).[64] [c] Measured at pH = 7.0, (Gabelin et al., 1982).[66] [d] Measured at pH = 7.0; upper value (Hurt et al., 1982);[62] lower value (Kramer and Crofts, 1994).[63] [e] A membrane of 50 Å thickness was assumed. Within the membrane, the dielectric constant was set to $\epsilon = 4$.

ence in the redox potentials is significantly smaller and the individual values are shifted toward the value in aqueous solution (Table 4).

Calculated Redox Potentials of the Hemes in the Whole Cbc_1 Complex. The values of the calculated redox potentials of the hemes in the native Cb are collected in Table 4 for three different pH values. The pH value of 6.6 was chosen for our computations, since the crystal structure of the Cbc_1 complex that we used was solved at that pH value. We calculated the redox potentials of the hemes from the Cb for the whole Cbc_1 complex assuming a solvent environment with a dielectric constant $\epsilon = 80$ outside of the protein complex. The obtained individual values of the redox potentials deviate form the corresponding experimental values at pH 7 by 32 meV or less. The calculated difference of the redox potentials of the two hemes is at pH 7 only 21 meV less than the experimental value. In good agreement with experiments[64,65] the redox potentials decrease with increasing pH value between 7 and 8 by 42 and 17 meV for the high and low potential hemes, respectively.

Calculated Redox Potentials of the Hemes in the Native Cb Subunit. If one compares the whole Cbc_1 complex with the C chain of the Cbc_1 complex carrying the Cb subunit (Figure 1) at pH 7 in a dielectric medium of $\epsilon = 80$, the calculated redox potential of the high potential heme H_h is 26 meV lower for the C chain, whereas the redox potential of the low potential heme H_l possesses practically the same value. This difference in the behavior of the high- and low-potential heme can be rationalized from the structure of the isolated Cb subunit, where the low potential heme remains well buried, whereas the high potential heme is partially exposed to the solvent. The stronger decrease of the redox potential of the high potential heme is in qualitative agreement with the measurements on the Cb subunit isolated from bovine heart (Table 4). However, the calculated redox potentials are about 35 meV higher than the corresponding experimental values of the native Cb isolated from the Cbc_1 complex. This discrepancy could be significant and may be due to differences between the conformation that the C chain adopts in the crystal structure of the whole Cbc_1 complex that was used for the computations and the conformation that the native Cb of the C chain isolated from the Cbc_1 complex assumes. Therefore, it is likely that in the later solution structure both hemes are more solvent-exposed than in the corresponding crystal structure of the Cb subunit. On the other hand, the difference of the redox potentials remains the same and agrees well with the corresponding experimental value for Cb isolated from the Cbc_1 complex.

To get an idea about the influence of the dielectric medium of the membrane on the redox potential of the hemes in the native Cb subunit, we calculated the redox potentials of the hemes in the Cb subunit, which is embedded in a dielectric layer of 50 Å thickness with $\epsilon = 4$. The Cb subunit was placed in the center of the layer. The normal of the layer was oriented parallel to the axes of the central four-helix bundle. With this arrangement the redox potentials increased at pH = 7 by about 55 meV with respect to the corresponding calculated values of the isolated Cb subunit in solution with $\epsilon = 80$, whereas the difference of the redox potentials practically did not change. We expect that the shift of redox potentials, which is due to the membrane, is smaller for the whole Cbc_1 complex, where both hemes are well buried inside the protein complex.

Since the dielectric medium of the membrane can be considered to have a similar influence on the isolated Cb subunit as the Cbc_1 complex, where the Cb subunit is embedded, we compare the calculated redox potentials with the measured values for the whole Cbc_1 complex. Interestingly, the redox potential of the high potential heme is for the Cb subunit in the membrane at pH = 6.6 slightly larger than the experimental value at pH = 7.0 and slightly below the experimental value for the whole Cbc_1 complex. But, at the same time, the redox potential of the low potential heme is for the Cb subunit in the membrane much larger than the experimental value of the whole Cbc_1 complex. Thus, the agreement of calculated and measured redox potential of the high potential heme of the Cb subunit in the membrane must be considered to be fortuitous.

Conclusions

The successful computation of the redox potentials of the two hemes in the artificial Cb suggests that the atomic coordinates of the artificial Cb generated by a modeling procedure are reliable. That means the model structure should have a quality, which is close to the quality of the crystal structure of a native protein. This is astonishing, since it is generally agreed that for native proteins a three-dimensional structure prediction does not work. In contrast to a native protein the artificial four-helix bundle protein that we considered here, possesses a much clearer building principle. The four helices are hold together by a template consisting in a cyclic decapeptide with a uniquely defined antiparallel β-strand structure instead of being sequentially connected by turns as would be the case for a single chain polypeptide. This clear separation between the helical and linker parts, makes it more certain that the helical polypeptides maintain their secondary structure. Furthermore, the template with its linker elements places the helices at relative positions to each other that are better defined as by use of turn structure elements that are part of a single polypeptide chain.

(66) Gabellini, N.; Bowyer, J. R.; Hurt, E.; Melandri, B. A.; Hauska, G. *Eur. J. Biochem.* **1982**, *126*, 105−111.
(67) Kraulis, P. J. *J. Appl. Crystallogr.* **1991**, *24*, 946−950.

With the exception of the four histidines, axially ligated to the two hemes, nearly half of each helix surface consists of hydrophobic residues, which form a large, uniform hydrophobic patch, whose face is oriented towards the center of the four-helix bundle. On the opposite side, each helix possesses a uniform hydrophilic patch, which is oriented towards the surface of the four-helix bundle. This specific distribution of hydrophobic and hydrophilic residues defines the orientation of the helices along their axes. The sequences of the two pairs of identical helices are especially constructed to host the two hemes. Two pairs of histidines at corresponding positions in a pair of oppositely oriented helices with identical sequences point toward each other and are ready to ligate the two hemes. The other helix pair possesses two pairs of glycines at positions where in the other helices the histidines are located. The glycines are needed to accommodate the bulky edges of the two hemes. All that makes this artificial Cb a structurally well-defined model system, where atomic coordinates can be generated from scratch by modeling procedures in a well-defined way.

We demonstrated that the atomic coordinates of this artificial four-helix bundle protein can be generated by a careful, stepwise modeling procedure. The essence of the tedious modeling protocol is to place the different molecular components as accurate as possible before one starts with a process of structural relaxation as for instance energy minimization. Details of the modeling procedure may serve as a guideline to generate atomic coordinates for similar artificial proteins. As a result, we obtained a strain free model structure of the artificial Cb that is very robust. This is demonstrated by analyzing the time evolution of RMS deviations of atomic coordinates obtained by MD simulations of the artificial Cb, which are as small as the one obtained under equivalent conditions for the native Cb subunit.

To test the atomic charges and the whole computational procedure for the evaluation of redox potentials in heme proteins without having the uncertainty of a modeled structure, we applied our methodology also to the hemes of the Cb subunit of the Cbc_1 protein complex from bovine heart. The obtained results are in good agreement with experimental values. However, the agreement between measured and calculated redox potentials was even better for the artificial Cb with deviations smaller than 15 meV. This may be fortuitous. The larger deviations for the native Cbc_1 complex may also be due to a sensibility of the measurements of the redox potentials of the hemes on preparation conditions of the Cbc_1 protein complex. Note that the values of the redox potential of the cytochrome b_6f complex from the same species measured in different labs can vary by as much as 20 meV (see Table 4). Such an influence may be much smaller for the artificial Cb. Another reason for large discrepancies between calculated and measured redox potentials of the hemes in the native Cb may be related to the quality of the atomic coordinates. Although the atomic coordinates of the artificial Cb are subject to considerable uncertainties due to the modeling procedure, the coordinates of the crystal structure of the Cbc_1 complex obtained at 3.0 Å resolution may also be uncertain to some extent.

The analysis of the factors determining the shifts in the redox potentials of the hemes in the artificial Cb yielded the following results. (1) The electrostatic coupling of the redox potentials of the two hemes is negligibly small. (2) Changing the dielectric medium from aqueous solution ($\epsilon = 80$ everywhere) to $\epsilon = 4$ within the protein volume, the redox potentials of both hemes are shifted by about the same amount. The change in the dielectric medium contributes about 45% to the total shift of the redox potentials of the two hemes. The remaining shift in the redox potentials is due to the special charge distribution in the artificial Cb protein. (3) The backbone charges contribute another 50% to the total shift of the redox potentials, but do not contribute to the difference between the redox potentials. (4) The charges of the hydrophilic residues contribute about 50% to the difference between the redox potential of the two hemes. However, at the same time they give rise to a negative contribution to the total shift of 20%. (5) The salt bridges that the arginines form with the propionic acids of the hemes shift the redox potential of the high potential heme (located near to the template) more than the low potential heme. Thus, they contribute about 50% to the difference and about 33% to the overall shift in the redox potential. (6) The template and the inner hydrophobic side chains contribute only marginally to shifts of the redox potentials of the hemes. Note that the contributions do not add up exactly to 100%, since these electrostatic energies are not exactly additive.

The present application demonstrates that atomic coordinates of an artificial protein with a clear building plan can be generated by appropriate modeling procedures. However, to test that the procedure really works it would be helpful to solve the structure also experimentally by crystal structure determination. The good agreement between calculated and measured redox potentials makes it possible to analyze the factors of the protein environment determining the shift in the redox potentials of hemes, which are cofactors in artificial and native proteins. That opens new avenues to understand how nature tunes redox potentials of cofactors in proteins that they can perform their function and how one can construct artificial proteins whose cofactors have desired redox potentials.

Appendix

Here, we only provide a short overview of the modeling steps that we applied. The code given in brackets refers to the modeling steps described in more detail in the Supporting Information.

In the first seven modeling steps we generated the atomic coordinates of the four helices (A1, A2), the two hemes (A4, A5) and the cyclic decapeptide (A6, A7) and assembled these molecular components to form the complete model of the artificial Cb as faithful as possible without using structural relaxation. The imidazole rings of the four histidines, which are axial ligands to the two hemes were arranged in an appropriate orientation by resetting the torsion angles and patched to the heme iron atom (A3). The cyclic decapeptide was patched to the four helices by thioether bonds involving the four cysteines of the decapeptide and the acetylated N-terminal Gly1 of the helices F and the acetylated side chains of the C-terminal Lys27 of the helices G (A7).

Next we applied a number of structural relaxation steps to the atomic coordinates of the artificial Cb. The molecular structure of the artificial protein resulting from the model building has still packing problems in particular with respect to the side chains. Possible strain and van der Waals clashes of atom pairs can be removed by energy minimization with appropriately applied constraining conditions using the CHARMM22[53] energy function. If a molecular structure put under strain is relaxed by energy minimization or MD simulation without applying constraints, the structural details that were carefully prepared by preceding modeling steps could get lost. Therefore, we applied different types of constraints to stabilize the molecular structure during the various phases of the structural relaxation as explained in more detail in the Support-

ing Information. Here, we list a short summary of the 10 different steps of structural relaxation, which we applied.

Before we started with the procedure of structural relaxation a number of constraints were set until the last but one relaxation step to keep the imidazole rings ligated to the hemes in the preset orientations and positions relative to the hemes in agreement with recent results on the imidazole heme orientations.[60] The side chain atoms of the four histidines were energy minimized with appropriate constraints (B1). The conformation of the salt bridges between the PR groups of the hemes and the four arginines of the helices F_1 and F_2 were adjusted by constraint energy minimization (B2). Next, we adjusted the side chain conformations of the two phenylalanines dividing the cavity of the four-helix bundle, which is hosting the two hemes in compartments of even size (B3). Now all side chains were relaxed by energy minimization first without the arginines, phenylalanines and cysteines and in a second relaxation step the side chains of the arginines and phenylalanines were also included (B4, B5). Then the cyclic decapeptide was energy minimized (B6, B7). With the following relaxation steps also the heme was allowed to move. We relaxed the conformations of the propionic acids and of the arginines forming salt bridges with the propionic acids (B8). Finally, we relaxed the whole artificial Cb by gradually reducing the constraints applied to the peptide backbone atoms (B9, B10). RMS deviations for the individual modeling steps are given in Table S1. The evolution of structural differences between the two hemes in the artificial Cb with the modeling steps are documented in Table S2.

Acknowledgment. We thank Dr. Donald Bashford and Dr. Martin Karplus for providing the programs MULTIFLEX and CHARMM22, respectively. Fruitful discussions with Dr. Wolfgang Haehnel are gratefully acknowledged. This work was supported by the Deutsche Forschungsgemeinschaft SFB 498 A5, the graduate colleges GRK 80/2 and GRK 268, by the Fonds der Chemischen Industrie and BMFT. S.D.Z. was supported by a DAAD fellowship.

Supporting Information Available: Description of the modeling steps to generate atomic coordinates of the artificial cytochrome b; RMS deviations of the structure of the artificial Cb for different modeling steps of the polypeptides in Table S1 and of the heme in Table S2; atomic partial charges of oxidized and reduced heme with two axially ligated imidazoles in Table S3; atomic partial charges of all titratable molecular groups in Table S4 (PDF). This material is available free of charge via the Internet at http://pubs.acs.org.

JA003878Z